Supporting Information for

Multiple Selectivity-Determining Mechanisms of H_2O_2 Formation in Iron Porphyrin-Catalysed Oxygen Reduction

Anna C. Brezny,[†,a,b] Hannah S. Nedzbala,[†,a] and James M. Mayer[*,a]

[a]Department of Chemistry, Yale University, New Haven, CT 06520, USA
[b]Department of Chemistry, Skidmore College, Saratoga Springs, NY 12866, USA

[†]These authors contributed equally.
*Corresponding Author, james.mayer@yale.edu

Table of Contents:

1. General

Iron(II) chloride (Sigma-Aldrich, >99%), *meso*-tetra(2,4,6-trimethylphenyl)porphyrin (TMP) (Frontier Scientific, >99%), *meso*-tetra(2-carboxyphenyl) porphine (2-COOH TPP) (Frontier Scientific), *meso*-tetra(2-carboxyphenyl) porphine methyl ester (2-COOMe TPP) (Frontier Scientific), *meso*-tetraphenyl porphine (TPP) (Frontier Scientific), *meso*-tetra(4-methoxyphenyl) porphine (4-OMe TPP) (Frontier Scientific), *para*-toluenesulfonic acid monohydrate (*p*-TsOH) (Sigma-Aldrich, >99%), sodium *para*-toluenesulfonate (*p*-TsONa) (Sigma Aldrich, 95%), trifluoroacetic acid (TFA) (Acros, 99%), sodium trifluoroacetate (Sigma-Aldrich, 98%), concentrated sulfuric acid (H_2SO_4) (Fisher, >95%), 2,6-ditertbutylpyridine (Sigma-Aldrich, 97%), tetrabutylammonium bisulfate ([NBu_4][HSO_4^-]) (Sigma Aldrich, 97%), 2,6-lutidine (Sigma-Aldrich, ReagentPlus®, 98%), lithium bis(trimethylsilyl)amide (LiHMDS) (Sigma Aldrich, 97%), aqueous hydrogen chloride (Macron, 38 wt. %), dichloromethane (DCM) (Fisher Scientific, ≥99.5%) magnesium sulfate (Fisher), thallium trifluoromethanesulfonate (Sigma-Aldrich, 97%), dioxygen (Airgas, Ultra High Purity) and deuterated chloroform (Cambridge Isotope Laboratories, 99.9%) were used as received without further purification.

Iron(II) bromide was gifted to us by the laboratory of Professor Patrick Holland as the bis-tetrahydrofuran adduct, which was prepared using a reported procedure.[1] The THF adduct was obtained by heating $FeBr_2$ in THF at 60 °C for 4 h; the solid was collected on a medium frit and the volatile materials were removed under vacuum.

N,*N*-Dimethylformamide (DMF) (Sigma-Aldrich, 99.8% anhydrous) and tetrahydrofuran (THF) (Fisher Scientific, unstabilized, 99.9%) were degassed with argon and dried using a Pure Process Technology solvent system. DMF was thoroughly sparged prior to use to remove trace dimethylamine.

Routine ^{1}H NMR spectra were recorded on Agilent 400 MHz or 500 MHz spectrometers and were referenced to residual protio solvent.

1.1. Synthesis of Fe(P)Cl

1.1.1. Fe(TMP)Cl

Iron(III) tetramesitylporphyrin chloride (Fe(TMP)Cl) and iron(III) tetramesitylporphyrin triflate ([Fe(TMP)][OTf]) were synthesized following the procedures for iron(III) tetraphenylporphyrin chloride and iron(III) tetraphenylporphyrin triflate, respectively.[2] The ^{1}H NMR and optical UV-vis spectra matched literature reports.[3]

1.1.2. Fe(2-COOH TPP)Cl

In a N_2-filled glovebox, *meso*-tetra(2-carboxyphenyl) porphine (10 mg, 0.0126 mmol, 1 equiv.), iron(II) chloride (32 mg, 0.252 mmol, 20 equiv.), and 2,6-lutidine (0.0074 mL, 0.0639 mmol, 5 equiv) were combined in 4 mL DMF. The mixture was refluxed at 160 °C for 18 hours under N_2. Upon cooling, 100 mL 1 M HCl(aq) was added, and the flask was sonicated briefly. The solution was cooled in an ice bath, the solid iron porphyrin precipitated, and was filtered (90% yield). The ^{1}H NMR spectrum of isolated Fe(2-COOH TPP)Cl matched literature reports.[3]

1.1.3. Fe(2-COOMe TPP)Cl

In a N_2-filled glovebox, LiHMDS (22 mg, 0.132 mmol) was added to a solution of *meso*-tetra(2-carboxyphenyl) porphine methyl ester (50 mg, 0.059 mmol) in 50 mL THF. The solution was stirred for approximately 10 minutes until color changed from deep violet to deep green. Subsequently, iron(II) bromide·$(THF)_2$ (22 mg, 0.061 mmol) was added. The solution quickly changed color to deep violet, and was allowed to stir for 30 minutes before the solvent was removed under vacuum. The solid was re-dissolved in dichloromethane and washed three times with 1 M HCl (aq) and one time with saturated $NaHCO_3$ (aq). The organic layer was removed under vacuum. The crude product was purified by flash column chromatography (99:1 DCM:MeOH) (84% yield). The ^{1}H NMR spectra of the isolated Fe(2-COOMe TPP)Cl matched literature reports.[3]

1.1.4. Fe(TPP)Cl

In a N_2-filled glovebox, LiHMDS (49 mg, 0.293 mmol) was added to a solution of *meso*-tetraphenyl porphine (100 mg, 0.163 mmol) in 50 mL THF. The solution was stirred for approximately 45 minutes until color changed from deep violet to deep green. Subsequently, iron(II) bromide·$(THF)_2$ (63 mg, 0.175 mmol) was added. The solution quickly changed color to deep violet, and allowed to stir for 30 minutes before the solvent was removed under vacuum. The solid was re-dissolved in dichloromethane and stirred vigorously with 1 M HCl (aq) for 30 minutes. The organic layer was removed under vacuum to afford a mixture of crude product and μ-oxo dimer. Mixture was redissolved in DCM and stirred vigorously with 1M KOH to afford the dimer, which was purified by flash column chromatography (99:1 DCM:MeOH). Stirred eluant vigorously with 3M HCl (aq) for 20 minutes to break up dimer and form desired product. The organic layer was removed under vacuum. The product was then recrystallized in DCM/pentane. (82% yield). ^{1}H NMR spectra of the isolated Fe(TPP)Cl match literature reports.[3]

1.1.5. Fe(4-OMe TPP)Cl

In a N_2-filled glovebox, *meso*-tetra(4-methoxyphenyl) porphine (113 mg, 0.153 mmol, 1 equiv.), iron(II) chloride 195 mg, 1.53 mmol, 10 equiv.), and 2,6-lutidine (0.178 mL, 1.53 mmol, 10 equiv.) were combined in 10 mL DMF. The mixture was refluxed at 160 °C for 24 hours under N_2. The reaction was cooled, exposed to air, and stirred for 5 minutes before removing the solvent under vacuum. The solid was re-dissolved in dichloromethane and washed four times with 0.1 M HCl (aq), three times with saturated $NaHCO_3$ (aq), and once with brine. The organic layer was dried over $MgSO_4$ before solvent was removed under vacuum. The crude product was purified by flash column chromatography (99:1 DCM:MeOH) and rewashed with conc. HCl. The solvent was removed under vacuum. The ^{1}H NMR spectrum of isolated Fe(2-COOH TPP)Cl matched literature reports.[3]

2. Derivation of Selectivity/[Reagent] Relationships

2.1. Competing Pathways for Water and Hydrogen Peroxide Formation[4]

Using the model proposed in Scheme S1 (reproduced from Scheme 1 in the main text), we derive the relationship between selectivity and the concentration of the exogenous acid.

Scheme S1. Kinetic model of generic bifurcation pathways from the Fe(P)(OOH) intermediate.[a]

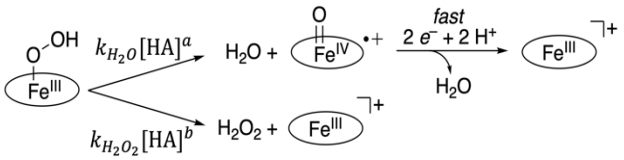

[a] Only pathways unimolecular in Fe(P) are considered in this Scheme (see Scheme S2).

The rate laws for formation of water and hydrogen peroxide are given by:

$$\frac{d[H_2O]}{dt} = 2k_{H_2O}[Fe(P)(OOH)][HA]^a \quad (S1)$$

and

$$\frac{d[H_2O_2]}{dt} = k_{H_2O_2}[Fe(P)(OOH)][HA]^b \quad (S2)$$

where a and b are the reaction orders in HA for these two elementary steps.

The selectivity (S) is defined as $[H_2O_2]/[H_2O]$, and by integrating the rate laws (with [HA] in excess and therefore constant), we obtain the relationship:

$$S = \frac{[H_2O_2]}{[H_2O]} = \frac{k_{H_2O_2}[HA]^b}{2k_{H_2O}[HA]^a} \quad (S3)$$

The log(S) is then described as:

$$\log(S) = \log\left(k_{H_2O_2}\right) + \log\left([HA]^b\right) - \log(2) - \log\left(k_{H_2O}\right) - \log([HA]^a) \quad (S4)$$

or

$$\log(S) = \log\left(k_{H_2O_2}\right) - \log\left(k_{H_2O}\right) + (b - a)\log([HA]) - \log(2) \quad (S5)$$

Taking a partial derivative with respect to log[HA], the correlation of selectivity and concentration of acid ([HA]) is defined with equation S6:

$$\frac{\partial \log(S)}{\partial \log([HA])} = b - a \quad (S6)$$

2.2.Non-Integer Slopes for Log(selectivity) versus Log([HA])

Using the kinetic model in **Scheme S2**, we derive the relationship between selectivity and the concentration of acid when formation of H_2O requires distal protonation, but H_2O_2 can be formed via the protonation, dissociation, or bimetallic pathways:

Scheme S2. Kinetic model for four bifurcation pathways from the Fe(P)(OOH) intermediate.

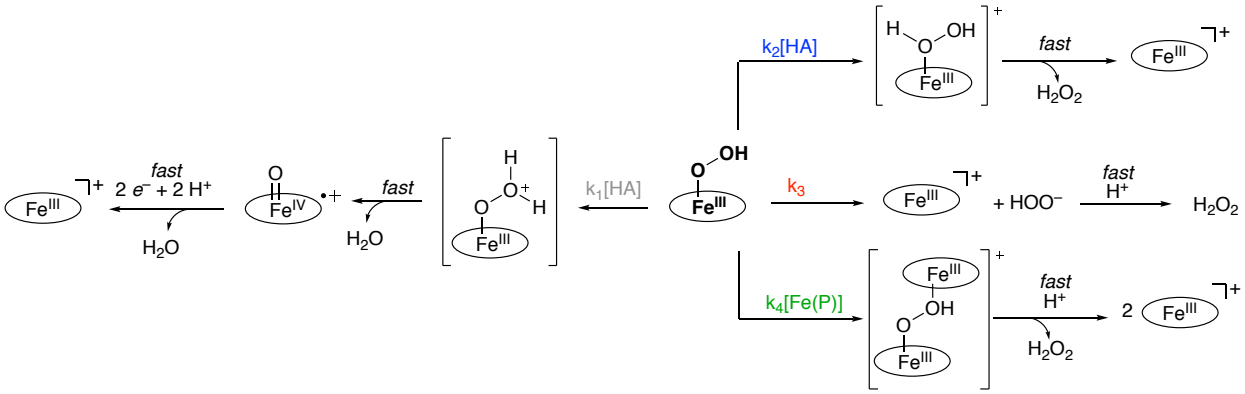

According to **Scheme S2**, the rate laws for formation of water and hydrogen peroxide are given by:

$$\frac{d[H_2O]}{dt} = 2k_1[Fe(P)(OOH)][HA] \quad (S7)$$

and

$$\frac{d[H_2O_2]}{dt} = [Fe(P)(OOH)](k_2[HA] + k_3 + k_4[Fe(P)]) \quad (S8)$$

The selectivity (S) is defined as $[H_2O_2]/[H_2O]$, and by integrating the rate laws, we obtain the relationship:

$$S = \frac{[H_2O_2]}{[H_2O]} = \frac{k_2[HA]+k_3+k_4[Fe(P)]}{2k_1[HA]} \quad (S9)$$

The log(S) is then described as:

$$\log(S) = \log(k_2[HA] + k_3 + k_4[Fe(P)]) - \log(2k_1) - \log([HA]) \quad (S10)$$

The partial derivative of equation S10 with respect to log[HA], can be defined by equation S11:

$$\frac{\partial \log(S)}{\partial \log([HA])} = \frac{\partial \log(S)}{\partial [HA]} \times \frac{\partial [HA]}{\partial \log([HA])} \quad (S11)$$

Using the definition for the derivative of a logarithm function (S12):

$$\frac{\partial \log([HA])}{\partial [HA]} = \frac{1}{[HA]*\ln 10} \quad (S12)$$

The inverse (equation S13), must also be true:

$$\frac{\partial [HA]}{\partial \log([HA])} = [HA] * \ln 10 \quad (S13)$$

The partial derivative of the log(S) with respect to [HA] gives:

$$\frac{\partial \log(S)}{\partial [HA]} = \frac{k_2}{(k_2[HA]+k_3+k_4[Fe(P)])\ln 10} - \frac{1}{[HA]*\ln 10} \quad \text{(S14)}$$

Substituting equations S13 and S14 into equation S11 gives:

$$\frac{\partial \log(S)}{\partial \log([HA])} = \frac{k_2[HA]}{k_2[HA]+k_3+k_4[Fe(P)]} - 1 \quad \text{(S15)}$$

When $k_2[HA] >> k_3 + k_4[Fe(P)]$ (i.e. when only the protonation pathway to give H_2O_2 is accessible):

$$\frac{\partial \log(S)}{\partial \log([HA])} = 0 \quad \text{(S16)}$$

When $k_3 + k_4[Fe(P)] >> k_2[HA]$ (i.e. when the dissociation or bimetallic pathways to give H_2O_2 are accessible):

$$\frac{\partial \log(S)}{\partial \log([HA])} = -1 \quad \text{(S17)}$$

When $k_2[HA]$, k_3, and $k_4[Fe(P)]$ are competitive (i.e. all pathways to H_2O_2 are operative), the plot of log(S) versus log([HA]) will have a non-integer, non-linear slope.

2.3.Non-Integer Slopes for Log(selectivity) versus Log([Fe(P)])

Using the definition of log(selectivity) (Equation S10) derived from the rate laws based on **Scheme S2** (see Section 2.2):

$$\log(S) = \log(k_2[HA] + k_3 + k_4[Fe(P)]) - \log(2k_1) - \log([HA]) \quad \text{(S10)}$$

The partial derivative of equation S10 with respect to log[Fe(P)], can be defined by equation S18:

$$\frac{\partial \log(S)}{\partial \log([Fe(P)])} = \frac{\partial \log(S)}{\partial [Fe(P)]} \times \frac{\partial [Fe(P)]}{\partial \log([Fe(P)])} \quad \text{(S18)}$$

Using the definition for the derivative of a logarithm function (S12):

$$\frac{\partial \log([Fe(P)])}{\partial [Fe(P)]} = \frac{1}{[Fe(P)]*\ln 10} \quad \text{(S19)}$$

The inverse (equation S13), must also be true:

$$\frac{\partial [Fe(P)]}{\partial \log([Fe(P)])} = [Fe(P)] * \ln 10 \quad \text{(S20)}$$

The partial derivative of the log(S) with respect to [HA] gives:

$$\frac{\partial \log(S)}{\partial [Fe(P)]} = \frac{k_4}{(k_2[HA]+k_3+k_4[Fe(P)])\ln 10} \quad \text{(S21)}$$

Substituting equations S20 and S21 into equation S18 gives:

$$\frac{\partial \log(S)}{\partial \log([Fe(P)])} = \frac{k_4[Fe(P)]}{k_2[HA]+k_3+k_4[Fe(P)]} \quad \text{(S22)}$$

When $k_4[Fe(P)] >> k_2[HA] + k_3$ (i.e. when only the bimetallic pathway to give H_2O_2 is accessible):

$$\frac{\partial \log(S)}{\partial \log([Fe(P)])} = 1 \quad \text{(S23)}$$

When $k_2[HA] + k_3 >> k_4[Fe(P)]$ (i.e. when only the dissociation or protonation pathways to give H_2O_2 are accessible):

$$\frac{\partial \log(S)}{\partial \log([Fe(P)])} = 0 \quad \text{(S24)}$$

When $k_2[HA]$, k_3, and $k_4[Fe(P)]$ are competitive (i.e. all pathways to H_2O_2 are operative), the plot of log(S) versus log([Fe(P)]) will have a non-integer, non-linear slope.

2.4. Fits to the Kinetic Model

The log(S) vs log([HA]) and log(S) vs log([Fe(P)] data collected for **2 - 5** are fit to the kinetic model shown in **Scheme S2**. The rate constants k_2, k_3, and k_4 were optimized using eq S15 and S22 to fit the catalytic data in **Figures S1** – **S4**. The resulting fits of the data are shown in **Figures S1** – **S4** and *preliminary* and *relative* rate constants are shown in **Table S1**. For the purpose of comparing relative rate constants, k_2 for each porphyrin was set to 1.

Table S1. *Preliminary* relative rate constants for selectivity determining steps in Fe(P) catalysed ORR, obtained from fitting to log(selectivity) vs log([HA]) and log(selectivity) vs log([Fe(P)]) data. Uncertainties in the relative values are ca. ±25%.

	Fe(2-COOH TPP)	**Fe(2-COOMe TPP)**	**Fe(TPP)**	**Fe(4-OMe TPP)**
k_2 ($M^{-1}s^{-1}$)	set to 1.0	set to 1.0	set to 1.0	set to 1.0
k_3 (s^{-1})	1×10^{-3}	1×10^{-6}	1×10^{-6}	6×10^{-3}
k_4 ($M^{-1}s^{-1}$)	2×10^{0}	3×10^{0}	1×10^{2}	4×10^{1}

When the relative rates for each of the three proposed H_2O_2 forming pathways are compared, the relative % H_2O_2 being produced from each of the three possible pathways can be predicted at different experimental conditions:

Table S2. Estimated contributions to the production of H_2O_2 from the three modelled pathways under different catalysis conditions.

	Fe(2-COOH TPP) % H_2O_2		**Fe(2-COOMe TPP) % H_2O_2**		**Fe(TPP) % H_2O_2**		**Fe(4-OMe TPP) % H_2O_2**	
	Low [HA] high [Fe(P)]	***Low [Fe(P)] high [HA]***	***Low [HA] high [Fe(P)]***	***Low [Fe(P)] high [HA]***	***Low [HA] high [Fe(P)]***	***Low [Fe(P)] high [HA]***	***Low [HA] high [Fe(P)]***	***Low [Fe(P)] high [HA]***
Protonation pathway	66 %	98 %	60 %	99 %	7 %	89%	10 %	88 %
Dissociation pathway	10 %	1 %	< 1 %	< 1 %	< 1 %	< 1 %	5 %	5 %
Bimetallic pathway	24 %	< 1 %	40 %	< 1 %	93 %	11 %	85 %	7 %

2.4.1. Fe(2-COOH TPP)

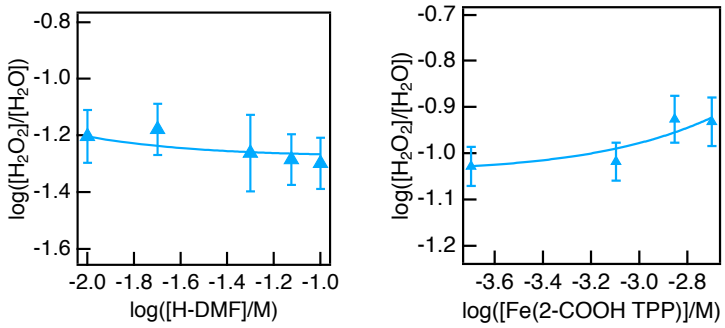

Figure S1. The data for log(selectivity) vs log[HA] (left) and log(selectivity) vs log[Fe(P)] (right) with Fe(2-COOH TPP) are fit to kinetic model shown in **Scheme S2**, with k_2 set to 1, $k_3 = 10 \times 10^{-3}$, and $k_4 = 2 \times 10^{0}$.

2.4.2. Fe(2-COOMe TPP)

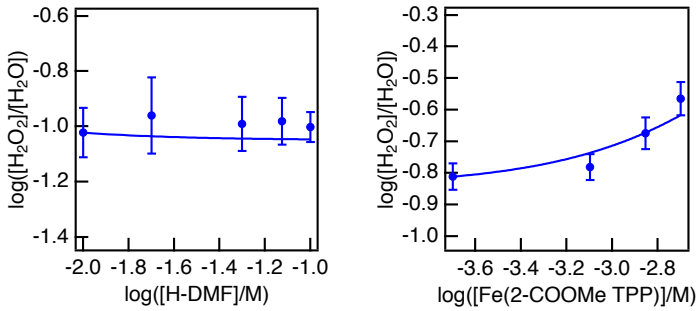

Figure S2. The data for log(selectivity) vs log[HA] (left) and log(selectivity) vs log[Fe(P)] (right) with Fe(2-COOMe TPP) are fit to kinetic model shown in **Scheme S2**, with k_2 set to 1, $k_3 = 1 \times 10^{-6}$, and $k_4 = 3 \times 10^{0}$.

2.4.3. Fe(TPP)

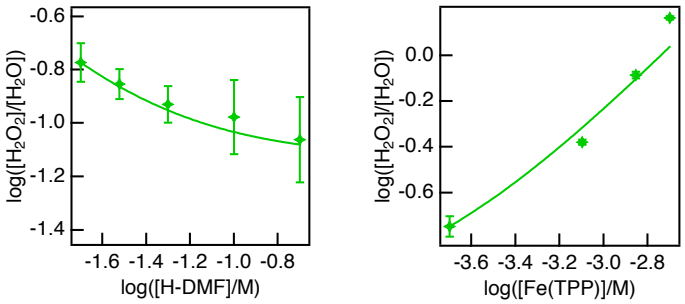

Figure S3. The data for log(selectivity) vs log[HA] (left) and log(selectivity) vs log[Fe(P)] (right) with Fe(TPP) are fit to kinetic model shown in **Scheme S2**, with k_2 set to 1, $k_3 = 1 \times 10^{-6}$, and $k_4 = 1 \times 10^{2}$.

2.4.4. Fe(4-OMe TPP)

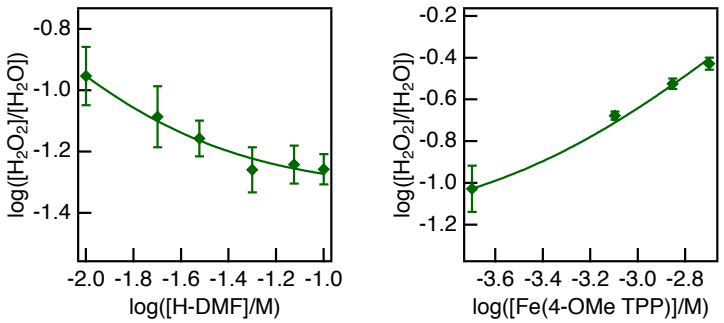

Figure S4. The data for log(selectivity) vs log[HA] (left) and log(selectivity) vs log[Fe(P)] (right) with Fe(4-OMe TPP) are fit to kinetic model shown in **Scheme S2**, with k_2 set to 1, $k_3 = 6 \times 10^{-3}$, and $k_4 = 4 \times 10^{1}$.

3. Cyclic Voltammetry

Cyclic voltammetry was conducted on CH Instruments potentiostats (models 600D/650D) using a 3 mm glassy carbon working electrode, a platinum auxiliary electrode, and a Ag pseudoreference electrode made using a CHI non-aqueous reference electrode kit. The silver wire was immersed in a jacketed compartment (separated from solution with a glass frit) containing 0.1 M [*n*-Bu_4N][PF_6] in DMF and allowed to equilibrate for 24 hours prior to use. Measurements were iR compensated for all experiments using built-in software to determine the resistance within the electrochemical window of interest ($E \approx E_{1/2}$). Resistance values typically measured < 100 Ohms. The glassy carbon working electrode was polished with 0.05 μm alumina on a Buehler felt pad between scans.

In the absence of dioxygen, all [Fe(P)]OTf displayed a chemically reversible $Fe^{III/II}$ couple. The scan rate dependence in the absence of O_2 demonstrated that current is proportional to the square root of scan rate ($v^{1/2}$),[2-4] consistent with a diffusion-limited process.

For kinetic cyclic voltammetry ORR experiments, a solution of [Fe(P)]OTf (0.2 mM) was prepared by combining Fe(P)Cl with 2 mM [Tl][OTf] in DMF containing 0.1 M [NBu_4][PF_6], and was analyzed in the presence of [HDMF]OTf. The solution was sparged with N_2 or Ar to measure the reversible $Fe^{III/II}$ couple. Subsequently, the solution was sparged with O_2 (1 atm) to measure the catalytic current under the same conditions. Current enhancement was observed with an onset corresponding to the $Fe^{III/II}$ couple.[2-4] Between scans, the working glassy carbon electrode was polished as described above and rinsed with DMF.

Qualitative comparison of rates under 1 atm air (0.7 mM O_2) vs. 1 atm O_2 (3.3 mM O_2) demonstrate that all porphyrins show a kinetic dependence on the concentration of O_2.[2-3,4] A rinse test confirmed that under catalytic conditions, adsorbed catalyst does not significantly contribute to the current (**Figure S5**, **Figure S6**, **Figure S8**, **Figure S9**). The electrochemical kinetics were calculated using foot-of-the-wave analysis (FOWA) for an EC′ mechanism as described previously.[3, 5] The foot region of the FOWA showed a linear dependence of normalized current (i_c/i_p) versus mole fraction of reduced catalyst,[2-4] implying a first-order dependence on [Fe^{II}(P)]. The catalytic rates all showed a first-order dependence on [HX].[2-4] Together these results indicate that the iron porphyrin catalysts explored follow the same mechanism as previously reported.[2]

Cyclic voltammograms of [Fe(2-COOMe TPP)]OTf in the presence of acid as compared to [Fe(2-COOH TPP)]OTf imply no hydrolysis of the methyl ester functional group under catalysis conditions (**Figure S7**).

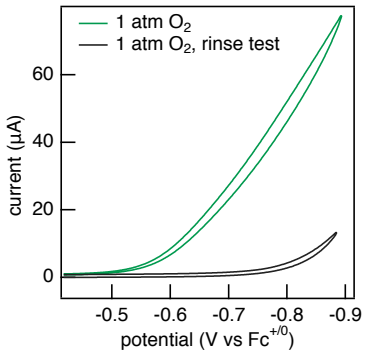

Figure S5. Cyclic voltammograms for the ORR catalyzed by [Fe(2-COOH TPP)]OTf in DMF under 1 atm O_2 in the presence of 0.1 M [NBu_4][PF_6] and 100 mM 1:1 *p*-TsOH:*p*-TsONa. The green trace is the catalytic wave in the solution containing soluble [Fe(2-COOH TPP)]OTf. The black trace is the same electrode rinsed with DMF and immersed in a solution containing no [Fe(2-COOH TPP)]OTf but with 0.1 M [NBu_4][PF_6] and 100 mM 1:1 *p*-TsOH:*p*-TsONa under 1 atm O_2.

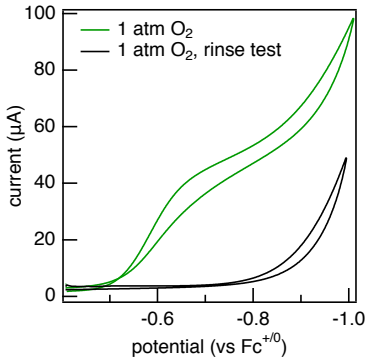

Figure S6. Cyclic voltammograms for the ORR catalyzed by [Fe(2-COOMe TPP)]OTf in DMF under 1 atm O_2 in the presence of 0.1 M [NBu_4][PF_6] and 100 mM 1:1 *p*-TsOH:*p*-TsONa. The green trace is the catalytic wave in the solution containing soluble [Fe(2-COOMe TPP)]OTf. The black trace is the same electrode rinsed with DMF and immersed in a solution containing no [Fe(2-COOMe TPP)]OTf but with 0.1 M [NBu_4][PF_6] and 100 mM 1:1 *p*-TsOH:*p*-TsONa under 1 atm O_2.

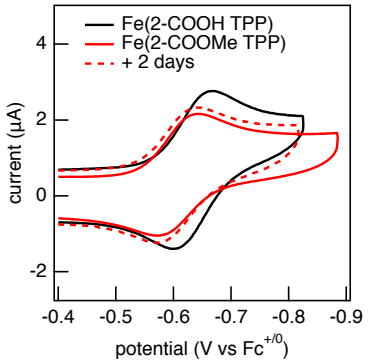

Figure S7. Cyclic voltammograms of [Fe(2-COOMe TPP)]OTf (red) and [Fe(2-COOH TPP)]OTf (black) demonstrating at even after two days no change in [Fe(2-COOMe TPP)]OTf $E_{1/2}$ (dashed red), thus no observable hydrolysis of methyl ester occurs. (0.2 mM iron porphyrin, 100 mM buffered *p*-TsOH, and 0.1 M [NBu_4][PF_6]).

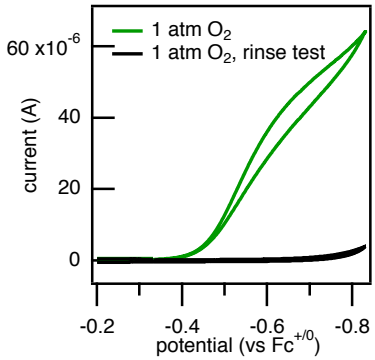

Figure S8. Cyclic voltammograms for the ORR catalyzed by [Fe(TPP)]OTf in DMF under 1 atm O_2 in the presence of 0.1 M [NBu_4][PF_6] and 200 mM [H-DMF][OTf]. The green trace is the catalytic wave in the solution containing soluble [Fe(TPP)]OTf. The black trace is the same electrode rinsed with DMF and immersed in a solution containing no [Fe(TPP)]OTf but with 0.1 M [NBu_4][PF_6] and 200 mM [H-DMF][OTf] under 1 atm O_2.

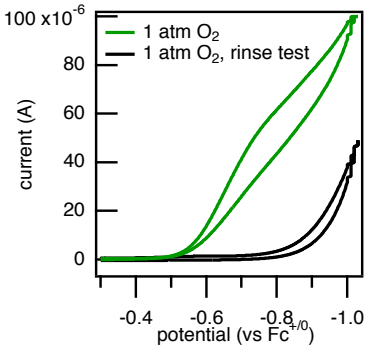

Figure S9. Cyclic voltammograms for the ORR catalyzed by [Fe(4-OMe TPP)]OTf in DMF under 1 atm O_2 in the presence of 0.1 M [NBu_4][PF_6] and 100 mM [H-DMF][OTf]. The green trace is the catalytic wave in the solution containing soluble [Fe(TPP)]OTf. The black trace is the same electrode rinsed with DMF and immersed in a solution containing no [Fe(4-OMe TPP)]OTf but with 0.1 M [NBu_4][PF_6] and 100 mM [H-DMF][OTf] under 1 atm O_2.

4. Rotating Ring-Disk Voltammetry

Rotating ring-disk voltammetry (RRDV) was conducted using a Pine Instruments rotator with either a Biologic VSP potentiostat or a BASi Epsilon potentiostat. Solutions were analyzed in a custom-built reservoir made from a 20 mL shot glass with a plastic top using a 5 mm glassy carbon (GC) disk electrode, Pt ring secondary working electrode, Pt auxiliary, and Ag pseudoreference electrode (prepared as described above). The Pt ring was electrochemically conditioned by cycling between +1 and –1 V (vs Ag/AgCl) in 0.5 M H_2SO_4. The GC disc and Pt ring working electrodes were polished separately on Buehler felt pads with 0.05 μm alumina. The collection efficiency was calculated to be 22% using ferrocene in DMF.[4]

For catalytic RRDV measurements, a 0.2 mM [Fe(P)]OTf solution was prepared by combining Fe(P)Cl with 2 mM [Tl][OTf] in 15 mL DMF with 0.1 M $[NBu_4]PF_6$ and the desired concentration of acid. The solution was sparged with O_2 for 10 minutes to ensure saturation. The disk was swept from –0.2 to –0.9 V vs $Fc^{+/0}$ at 20 mV/s. The ring was held at +0.6 V versus $Fc^{+/0}$ or greater to oxidize H_2O_2 produced at the disk. More oxidizing potentials did not impact the ring currents. Experiments were collected in the absence of ferrocene, but it was added at the end of the experiment as an internal reference. Fe(P) displayed Levich behavior in the absence of O_2. Consistent with current being limited by chemical steps under catalytic conditions, non-Levich behavior was observed in the presence of dioxygen. Additionally, traces do not show expected S-shape due to background direct oxygen reduction occurring at the electrode at more negative potentials. (**Figure S11**, **Figure S14**, **Figure S17**, **Figure S20**). Data for [Fe(TMP)]OTf previously reported.[4]

4.1. $\%H_2O_2$ Calculation

The $\%H_2O_2$ was calculated using equation S25, where *N* is the collection efficiency of the setup (22%). The $\%H_2O_2$ was calculated and averaged over a range of disk potentials after catalytic onset and before background ORR (approximately –0.60 to –0.70 V vs $Fc^{+/0}$).

$$\%\, H_2O_2 = \frac{100\frac{2i_{ring}}{N}}{i_{disk}+\frac{i_{ring}}{N}} \tag{S25}$$

4.2. Measured Selectivity

Control experiments varying the ring potential indicate that measured ring current is due to oxidation of H_2O_2, not unreacted Fe^{II}(P) formed at the disk (**Figure S10**, **Figure S13**, **Figure S16**, **Figure S19**). Control experiments varying the concentration of Fe(P)OTf from 0.2–2.0 mM were collected at the lowest concentration of [H-DMF][OTf] used under catalytic conditions (**Figure S15**, **Figure S18**, **Figure S21**). Previously reported data for Fe(TMP)OTf demonstrate no effect of [Fe] on measured selectivity.[4]

4.2.1. Fe(2-COOH TPP)

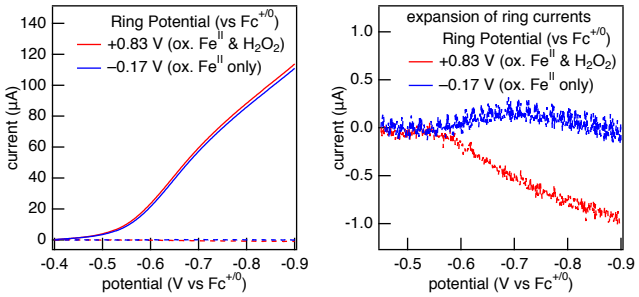

Figure S10. RRDV traces of ~0.2 mM [Fe(2-COOH TPP)]OTf under 1 atm of O_2 with 10 mM *p*-TsOH in DMF containing 0.1 M [NBu_4][PF_6]. Disk swept cathodically and ring potential set to either +0.83 V (red) or –0.17 V (blue) versus $Fc^{+/0}$. At –0.17 V Fe^{II}(2-COOH TPP) can be oxidized to [Fe^{III}(2-COOH TPP)]OTf, but H_2O_2 is not oxidized. No substantial ring current was observed when the ring was held at –0.17 V, indicating that H_2O_2, not Fe^{II}(2-COOH TPP), is the source of the ring current when the Pt ring is set to 0.83 V. Reactions with *p*-TsOH are slower than those with [H-DMF][OTf].[4, 6] Thus, if rates with Fe^{II}(2-COOH TPP) and *p*-TsOH are fast enough that the ring current is not due to Fe^{II}(TMP) re-oxidation, we can assume the same is true with the stronger [H-DMF][OTf] acid.

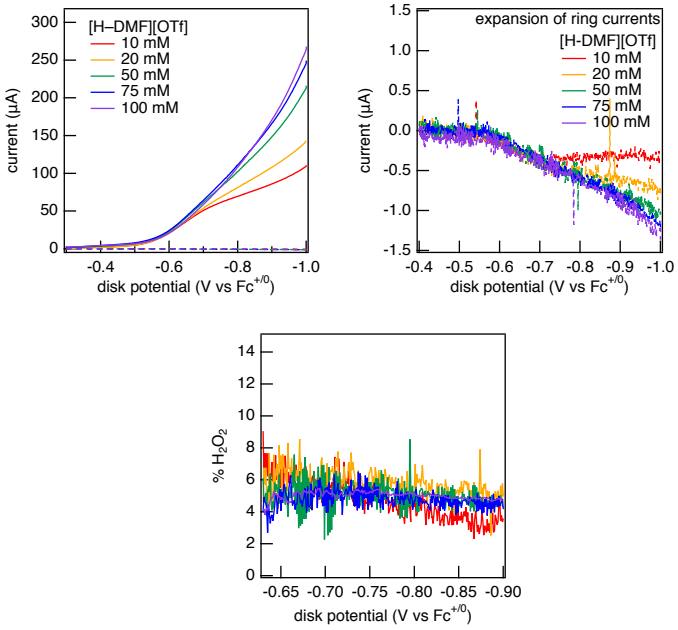

Figure S11. Top: RRDV traces of ~0.2 mM [Fe(2-COOH TPP)]OTf under 1 atm of O_2 with varied concentrations of [H-DMF][OTf] in DMF containing 0.1 M [NBu_4][PF_6] rotating at 3000 RPM. Disk swept cathodically and ring potential set to 0.6 V versus $Fc^{+/0}$. Bottom: Measured % H_2O_2 as a function of disk potential under the same conditions.

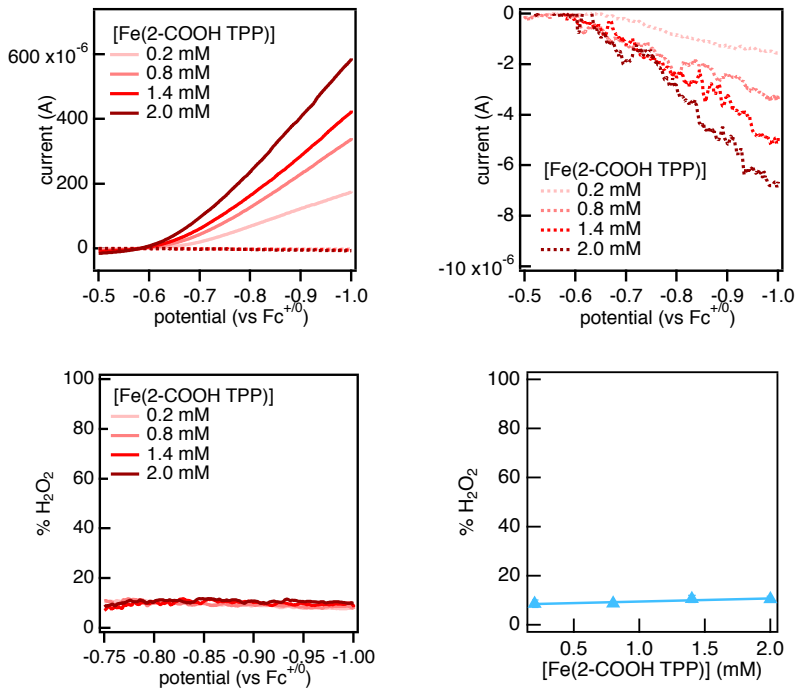

Figure S12. Top: RRDV traces of varying concentrations of [Fe(2-COOH TPP)]OTf under 1 atm O_2 at 20 mM [H-DMF][OTf] in DMF containing 0.1 M [NBu_4][PF_6] rotating at 3000 RPM. Disk swept cathodically and ring potential set to 0.6 V versus $Fc^{+/0}$. Bottom left: Measured % H_2O_2 as a function of disk potential under the same conditions. Bottom right: %H_2O_2 plotted as a function of [Fe(2-COOH TPP)]. %H_2O_2 does not change significantly with respect to [Fe(2-COOH TPP)][OTf].

4.2.2. Fe(2-COOMe TPP)

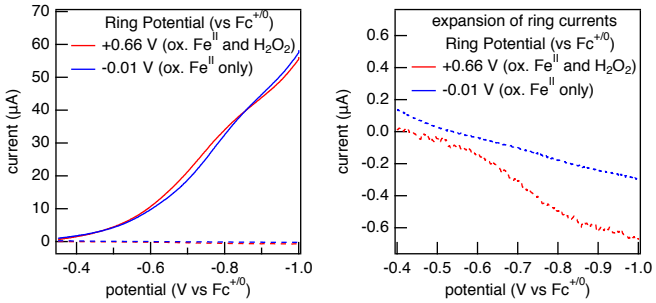

Figure S13. RRDV traces of ~0.2 mM [Fe(2-COOMe TPP)]OTf under 1 atm of O_2 with 10 mM *p*-TsOH in DMF containing 0.1 M [NBu_4][PF_6]. Disk swept cathodically and ring potential set to either +0.66 V (red) or –0.01 V (blue) versus $Fc^{+/0}$. At –0.01 V Fe^{II}(2-COOMe TPP) can be oxidized to [Fe^{III}(2-COOMe TPP)]OTf, but H_2O_2 is not oxidized. No substantial ring current was observed when the ring was held at –0.01 V, indicating that H_2O_2, not Fe^{II}(2-COOMe TPP), is the source of the ring current when the Pt ring is set to 0.66 V. Reactions with *p*-TsOH are slower than those with [H-DMF][OTf].[4, 6] Thus, if rates with Fe^{II}(2-COOH TPP) and *p*-TsOH are fast enough that the ring current is not due to Fe^{II}(TMP) re-oxidation, we can assume the same is true with the stronger [H-DMF][OTf] acid.

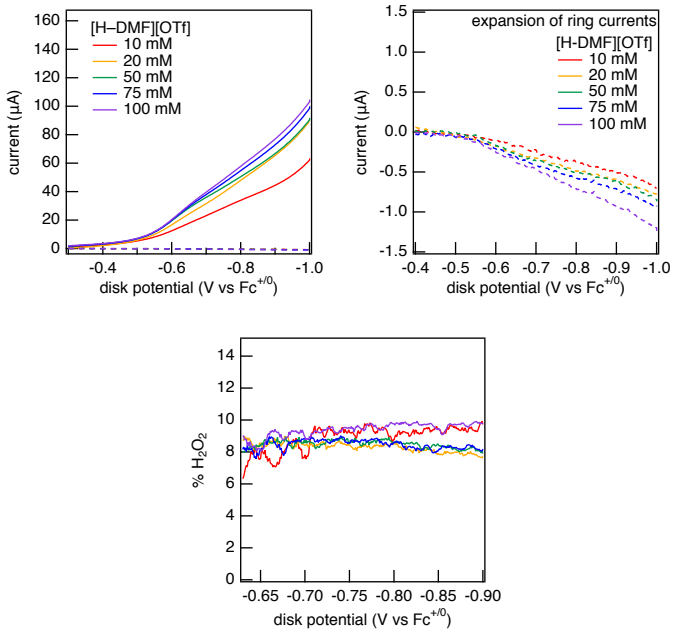

Figure S14. Top: RRDV traces of ~0.2 mM [Fe(2-COOMe TPP)]OTf under 1 atm of O_2 with varied concentrations of [H-DMF][OTf] in DMF containing 0.1 M [NBu_4][PF_6] rotating at 3000 RPM. Disk swept cathodically and ring potential set to 0.6 V versus $Fc^{+/0}$. Bottom: Measured % H_2O_2 as a function of disk potential under the same conditions.

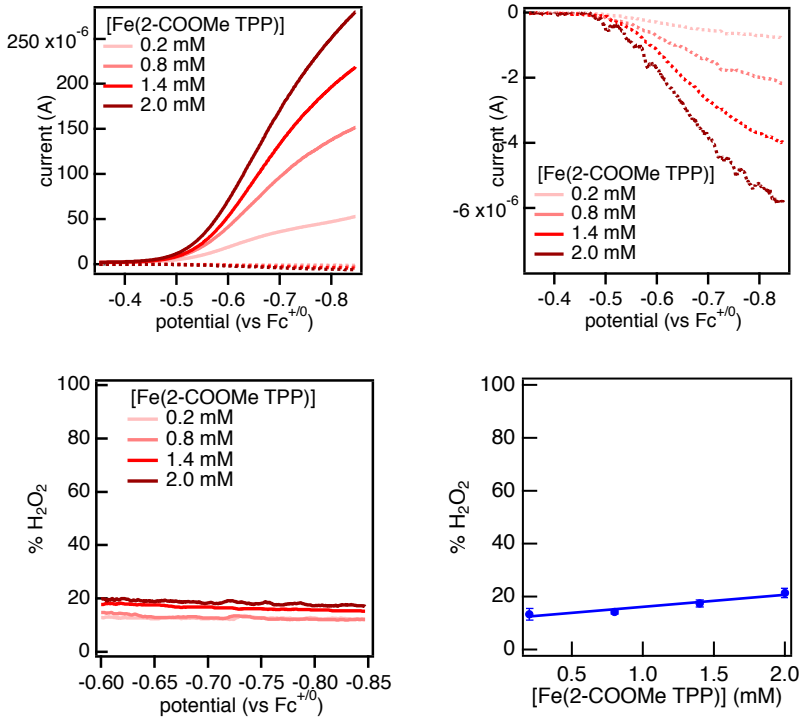

Figure S15. Top: RRDV traces of varying concentrations of [Fe(2-COOMe TPP)]OTf under 1 atm O_2 at 10 mM [H-DMF][OTf] in DMF containing 0.1 M [NBu_4][PF_6] rotating at 3000 RPM. Disk swept cathodically and ring potential set to 0.6 V versus $Fc^{+/0}$. Bottom left: Measured % H_2O_2 as a function of

disk potential under the same conditions. Bottom right: $\%H_2O_2$ plotted as a function of [Fe(2-COOMe TPP)]. $\%H_2O_2$ does not change significantly with respect to [Fe(2-COOMe TPP)][OTf].

4.2.3. Fe(TPP)

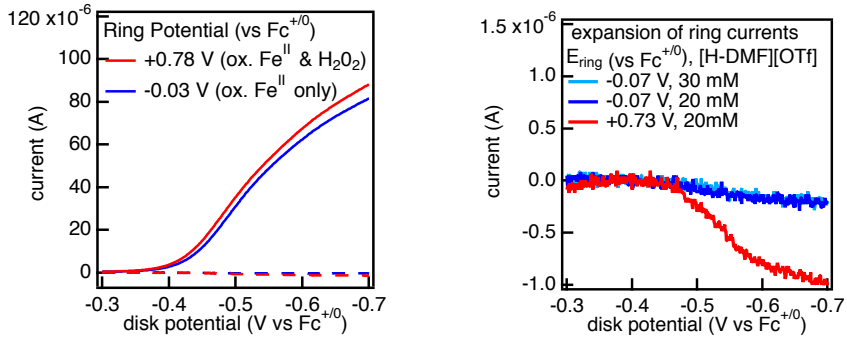

Figure S16. Left: RRDV traces of ~0.2 mM [Fe(TPP)]OTf under 1 atm of O_2 with 20 mM [H-DMF][OTf] in DMF containing 0.1 M [NBu_4][PF_6]. Disk swept cathodically and ring potential set to either +0.73 V (red) or –0.07 V (blue) versus $Fc^{+/0}$. At –0.07 V Fe^{II}(TPP) can be oxidized to [Fe^{III}(TPP)]OTf, but H_2O_2 is not oxidized. No substantial ring current was observed when the ring was held at –0.07 V, indicating that H_2O_2, not Fe^{II}(TPP), is the source of the ring current when the Pt ring is set to 0.73 V.

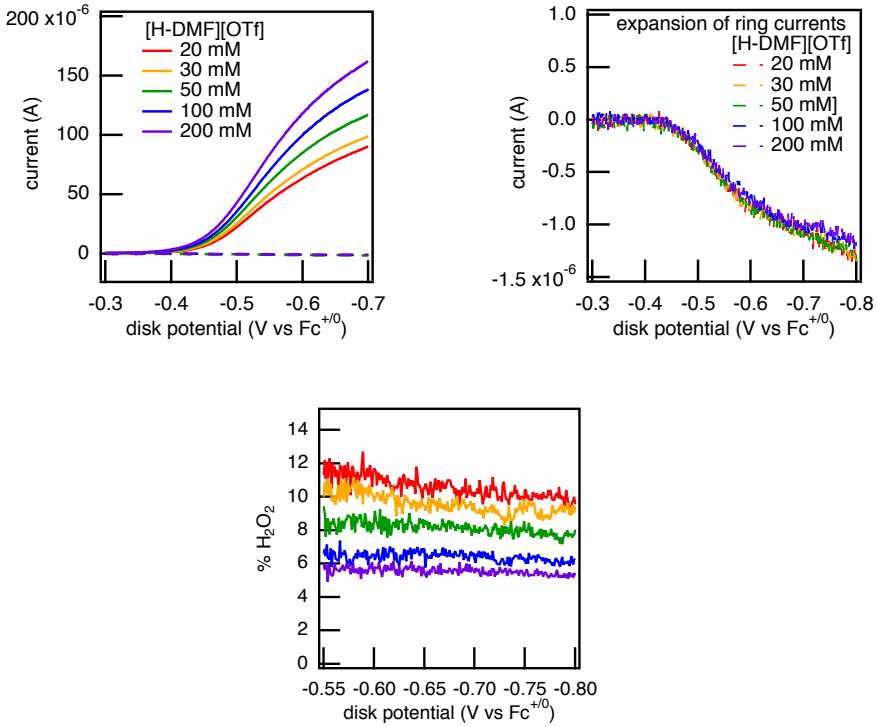

Figure S17. Top: RRDV traces of ~0.2 mM [Fe(TPP)]OTf under 1 atm of O_2 with varied concentrations of [H-DMF][OTf] in DMF containing 0.1 M [NBu_4][PF_6] rotating at 3000 RPM. Disk swept cathodically and ring potential set to 0.6 V versus $Fc^{+/0}$. Bottom: Measured % H_2O_2 as a function of disk potential under the same conditions.

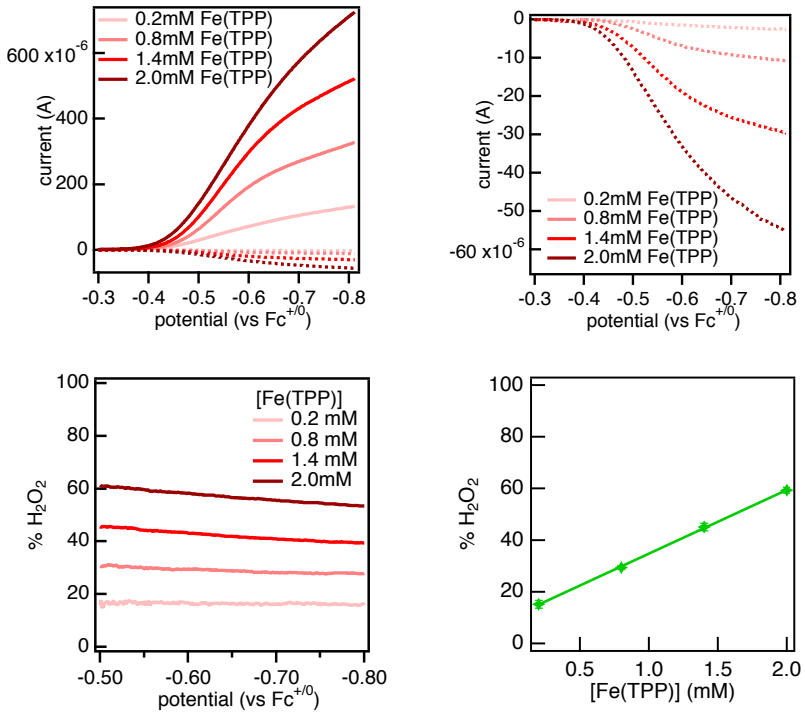

Figure S18. Top: RRDV traces of varying concentrations of [Fe(TPP)]OTf under 1 atm O_2 at 20 mM [H-DMF][OTf] in DMF containing 0.1 M [NBu_4][PF_6] rotating at 3000 RPM. Disk swept cathodically and ring potential set to 0.6 V versus $Fc^{+/0}$. Bottom: Measured % H_2O_2 as a function of disk potential under the same conditions. Bottom right: %H_2O_2 plotted as a function of [Fe(TPP)]. %H_2O_2 changes significantly with respect to [Fe(TPP)][OTf].

4.2.4. Fe(4-OMe TPP)

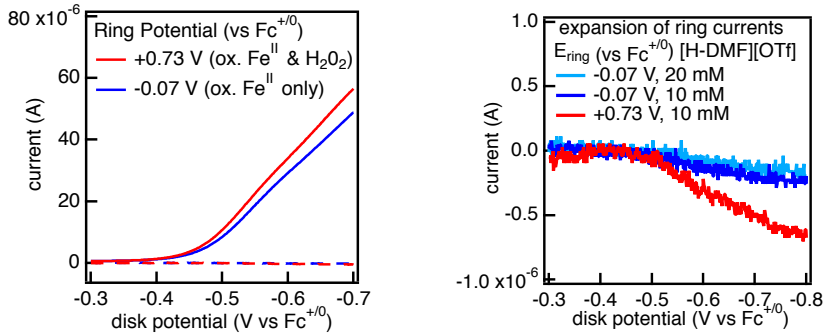

Figure S19. RRDV traces of ~0.2 mM [Fe(4-OMe TPP)]OTf under 1 atm of O_2 with 10 mM [H-DMF][OTf] in DMF containing 0.1 M [NBu_4][PF_6]. Disk swept cathodically and ring potential set to either +0.73 V (red) or –0.07 V (blue) versus $Fc^{+/0}$. At –0.07 V Fe^{II}(4-OMe TPP) can be oxidized to [Fe^{III}(4-OMe TPP)]OTf, but H_2O_2 is not oxidized. No substantial ring current was observed when the ring was held at –0.07 V, indicating that H_2O_2, not Fe^{II}(4-OMe TPP), is the source of the ring current when the Pt ring is set to 0.73 V.

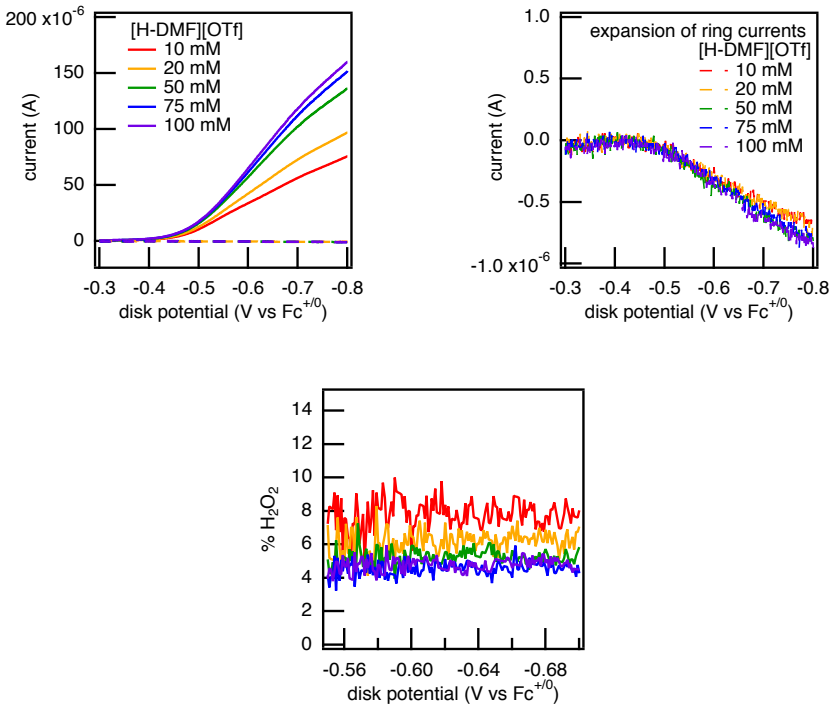

Figure S20. Top: RRDV traces of ~0.2 mM [Fe(4-OMe TPP)]OTf under 1 atm of O_2 with varied concentrations of [H-DMF][OTf] in DMF containing 0.1 M [NBu_4][PF_6] rotating at 3000 RPM. Disk swept cathodically and ring potential set to 0.6 V versus $Fc^{+/0}$. Bottom: Measured % H_2O_2 as a function of disk potential under the same conditions.

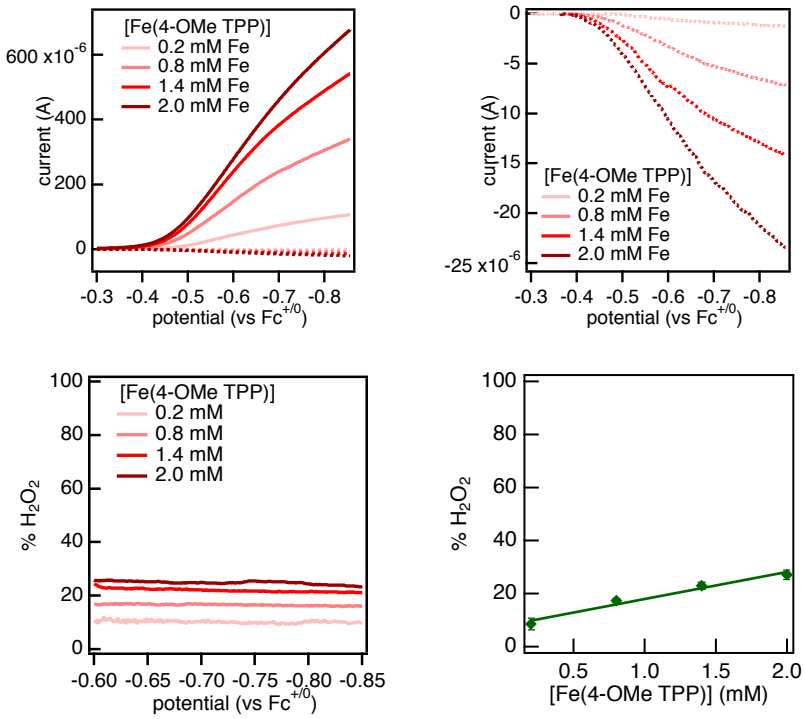

Figure S21. Top: RRDV traces of varying concentrations of [Fe(4-OMe TPP)]OTf under 1 atm O_2 at 10 mM [H-DMF][OTf] in DMF containing 0.1 M [NBu_4][PF_6] rotating at 3000 RPM. Disk swept cathodically and ring potential set to 0.6 V versus $Fc^{+/0}$. Bottom left: Measured % H_2O_2 as a function of disk potential under the same conditions. Bottom right: %H_2O_2 plotted as a function of [Fe(TPP)]. %H_2O_2 changes with respect to [Fe(4-OMe TPP)][OTf].

4.3. Rotation Rate Effects

4.3.1. Fe(2-COOH TPP)

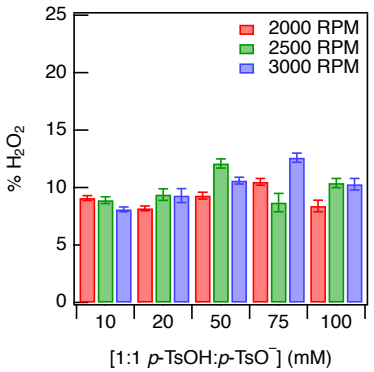

Figure S22. Measured %H_2O_2 versus concentration of acid at several rotation rates for Fe(2-COOH TPP). The measured ring current is independent of rotation rate at all acid concentrations.

4.3.2. Fe(2-COOMe TPP)

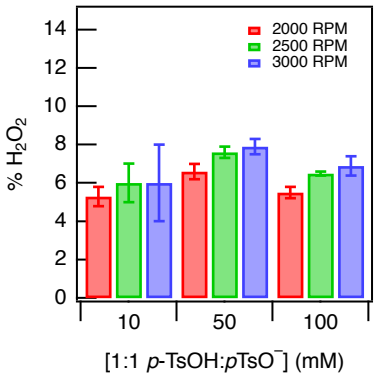

Figure S23. Measured $\%H_2O_2$ versus concentration of acid at several rotation rates for Fe(2-COOH TPP). The measured ring current is independent of rotation rate at all acid concentrations.

4.3.3. Fe(TPP)

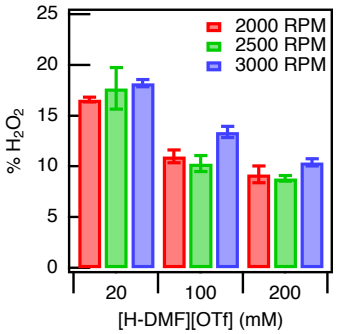

Figure S24. Measured $\%H_2O_2$ versus concentration of acid at several rotation rates for Fe(TPP). The measured ring current is roughly independent of rotation rate at all acid concentrations. While the $\%H_2O_2$ values at 3000 RPM for the 100 and 200mM solutions are slightly higher than those observed at slower rotation speeds, these differences are not significant when compared to typical rotation rate dependences such as those observed with Fe(TMP).[4]

4.3.4. Fe(4-OMe TPP)

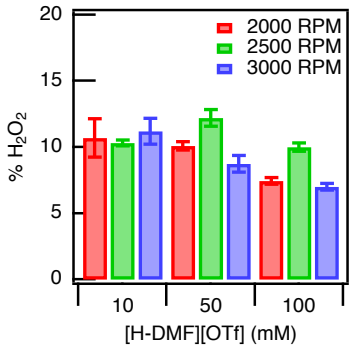

Figure S25. Measured $\%H_2O_2$ versus concentration of acid at several rotation rates for Fe(4-OMe TPP). The measured ring current is independent of rotation rate at all acid concentrations.

5. ORR Overpotential Comparison

The overpotential (η) for a molecular catalyst for the ORR is defined as the difference between the thermodynamic potential for O_2/H_2O under the relevant catalytic conditions (E_{ORR}) and the reduction potential of the catalyst ($E_{1/2}$) (equation S26).[7-8] The thermodynamic potential, E_{ORR}, be estimated using the standard potential for O_2/H_2O in organic solvents[9] and the application of the Nernst equation to account for non-standard state experimental conditions. The $E_{1/2}$ values for the catalysts explored in this work are within 100 mV of each other (–0.530 to –0.630 V). Therefore, under a given set of conditions, the overpotentials of all catalysts are within 100 mV.

$$\eta = E_{ORR} - E_{1/2} \quad \text{(S26)}$$

Based on previous studies from our group,[3] solutions were estimated to contain 20±10 mM H_2O using Karl Fischer titration methods. A difference of 20 mM H_2O (10 vs 30 mM) leads to an error of ~14 mV in overpotential.

6. References

1. Winter, G.; Thompson, D. W.; Loehe, J. R., Iron(II) Halides. In *Inorg. Synth.*, Wold, A.; Ruff, J. K., Eds. 1973; pp 99-104.
2. Pegis, M. L.; Martin, D. J.; Wise, C. F.; Brezny, A. C.; Johnson, S. I.; Johnson, L. E.; Kumar, N.; Raugei, S.; Mayer, J. M., Mechanism of Catalytic O_2 Reduction by Iron Tetraphenylporphyrin. *J. Am. Chem. Soc.* **2019,** *141*, 8315-8326.
3. Pegis, M. L.; McKeown, B. A.; Kumar, N.; Lang, K.; Wasylenko, D. J.; Zhang, X. P.; Raugei, S.; Mayer, J. M., Homogenous Electrocatalytic Oxygen Reduction Rates Correlate with Reaction Overpotential in Acidic Organic Solutions. *ACS Cent. Sci.* **2016,** *2*, 850-856.
4. Brezny, A. C.; Johnson, S. I.; Raugei, S.; Mayer, J. M., Selectivity-Determining Steps in O_2 Reduction Catalyzed by Iron(tetramesitylporphyrin). *J. Am. Chem. Soc.* **2020,** *142*, 4108-4113.
5. Costentin, C.; Drouet, S.; Robert, M.; Savéant, J.-M., Turnover Numbers, Turnover Frequencies, and Overpotential in Molecular Catalysis of Electrochemical Reactions. Cyclic Voltammetry and Preparative-Scale Electrolysis. *J. Am. Chem. Soc.* **2012,** *134*, 11235-11242.
6. Pegis, M. L.; Wise, C. F.; Koronkiewicz, B.; Mayer, J. M., Identifying and Breaking Scaling Relations in Molecular Catalysis of Electrochemical Reactions. *J. Am. Chem. Soc.* **2017,** *139*, 11000-11003.
7. Appel, A. M.; Helm, M. L., Determining the Overpotential for a Molecular Electrocatalyst. *ACS Catal.* **2014,** *4*, 630-633.
8. Rountree, E. S.; McCarthy, B. D.; Eisenhart, T. T.; Dempsey, J. L., Evaluation of homogeneous electrocatalysts by cyclic voltammetry. *Inorg. Chem.* **2014,** *53*, 9983-10002.
9. Pegis, M. L.; Roberts, J. A.; Wasylenko, D. J.; Mader, E. A.; Appel, A. M.; Mayer, J. M., Standard Reduction Potentials for Oxygen and Carbon Dioxide Couples in Acetonitrile and N,N-Dimethylformamide. *Inorg. Chem.* **2015,** *54*, 11883-11888.